Trapping cold atoms near carbon nanotubes: Thermal spin flips and Casimir-Polder potential

R. Fermani,* S. Scheel, and P. L. Knight
Quantum Optics and Laser Science, Blackett Laboratory, Imperial College London, Prince Consort Road, London SW7 2AZ, United Kingdom
(Received 23 March 2007; published 28 June 2007)

We investigate the possibility of trapping ultracold ^{87}Rb atoms near the outside of a metallic carbon nanotube, which we imagine using as a miniaturized current-carrying wire. We calculate atomic spin-flip lifetimes and compare the strength of the Casimir-Polder potential with the magnetic trapping potential. Our analysis indicates that the Casimir-Polder force is the dominant loss mechanism, and we compute the minimum distance to the carbon nanotube at which the atoms can be trapped to be larger than 100 nm.

DOI: 10.1103/PhysRevA.75.062905 PACS number(s): 34.50.Dy, 42.50.Ct, 78.67.Ch, 03.75.Be

I. INTRODUCTION

Advances in magnetic trapping of clouds of ultracold atoms and Bose-Einstein condensates have received considerable research attention [1–4]. The control and manipulation of atomic clouds is of fundamental importance in the investigation of the basic physical properties of atom-surface interaction [5–7], as well as in quantum-information processing [8,9]. As trapped cold atoms appear to be very sensitive to magnetic-field variations, they represent a powerful tool in magnetic-field imaging as well as in gaining insight into atom-surface coupling phenomena [10,11]. The challenge is to keep the atoms as close as possible to the substrate material to map the magnetic and electric fields in the vicinity of the surface. The combination of quantum state control with the development of ever smaller magnetic traps is an essential element in the implementation of integrated quantum devices for fundamental research, quantum-information processing, and precision measurement.

Along with the push toward miniaturization evolved the idea of devising even smaller structures based on carbon nanotubes (CNs) [12]. Carbon nanotubes are carbon monolayers rolled up into cylinders of a few nanometers diameter [13,14]. They have been widely investigated theoretically and experimentally as they play a key role in miniaturized electronic, mechanical, electromechanical, and scanning-probe devices. For their potential use as miniaturized current-carrying wires, it is important to realize that the desired close proximity of a neutral atom and the carbon atoms that make up the nanotube can vastly enhance the influence of dispersion forces, and we address this point in this paper.

It is well known that an atom held in a magnetic trap near an absorbing dielectric surface will be subject to thermally induced spin-flip transitions whose origin lies in fluctuating magnetic fields, which can be attributed to resistive noise in the substrate [15,16]. In accordance with the fluctuation-dissipation theorem, dissipation processes associated with a finite conductivity give rise to electromagnetic-field fluctuations. These fluctuations can be strong enough to drive spin transitions that lead to trapping losses [17–19].

In addition, an atom placed near a dielectric body will experience a dispersion force due to the presence of the dielectric material—the Casimir-Polder force [20–23]. The potential generating this force adds to the magnetic trapping potential and may cause the trap to become unstable at small distances.

With this in mind, CNs seem to represent rather attractive structures for designing miniaturized magnetic traps. This is, on one hand, due to the fact that they consist of a very small amount of dielectric matter which means that unwanted dispersion forces such as the Casimir-Polder force are minimized. On the other hand, they also possess extremely homogeneous surfaces and are thus less likely to induce inhomogeneities in the potential surface of the trap.

This paper is organized as follows. In Sec. II we introduce the basic concepts of magnetic trapping of neutral atoms. In Sec. III the spin-flip lifetime is calculated and compared to the tunneling lifetime resulting from the combination of the magnetic trapping potential and the Casimir-Polder potential. Both lifetimes are given in terms of the dyadic Green tensor. In order not to interrupt the flow of arguments and results we will present technical details about the conductivity and the Green tensor for a single-wall CN in the Appendices. Some conclusions are drawn in Sec. IV.

II. MAGNETIC TRAPS FOR NEUTRAL ATOMS

In this section, we briefly review magnetic trapping using straightforward tools of electromagnetism. An atom with a magnetic dipole moment $\boldsymbol{\mu}$ placed in a magnetic field $\mathbf{B}_T$ experiences an interaction potential

$$V = -\boldsymbol{\mu} \cdot \mathbf{B}_T. \tag{1}$$

Assuming that a low-field-seeking atom is in the state $|IJFm_F\rangle$, Eq. (1) corresponds to a Zeeman energy $V = g_F \mu_B m_F B$ that depends on the quantum number m_F and on the magnitude of the field $B = |\mathbf{B}_T|$, while it is independent of the field's direction, with g_F the Landé factor and μ_B the Bohr magneton.

Let us consider a current I flowing through a wire along the z direction that generates a circular magnetic field $\mathbf{B}$. Applying a homogeneous bias magnetic field $\mathbf{B}_b$ pointing in a direction orthogonal to the wire, a line of vanishing magnetic field parallel to the wire is created which is located a distance $y_0 = \mu_0 I/(2\pi B_b)$ away from the wire. The total field is given by $\mathbf{B}_T = \mathbf{B} + \mathbf{B}_b$, whose gradient $B'(r) = -\mu_0 I/(2\pi r^2)$,

*Electronic address: rachele.fermani@imperial.ac.uk

at the position of the field minimum y_0, can be written as $B'(y_0)=b'=-2B_b^2\pi/(\mu_0 I)$. As $B'(y_0)$ is independent of position, the superposition of the magnetic field created by the wire and the homogeneous bias field creates a two-dimensional quadrupole-type trap [24]. In such a trap, the trapping potential can be approximated by a linear function of the magnetic field gradient b'. The magnetic field can be expressed as $\mathbf{B}=b'x\mathbf{e}_x-b'y\mathbf{e}_y$ and its modulus is $|\mathbf{B}|=b'(x^2+y^2)^{1/2}=b'r$ with r denoting the distance from the trap center.

The modulus of the y component of $\mathbf{B}_T$ vanishes at the trap center. In order to prevent Majorana transitions to nontrapped magnetic levels, a further offset field $\mathbf{B}_o$ parallel to the wire is applied with $|\mathbf{B}_o| \ll |\mathbf{B}|$. The magnitude of the field near the center of the trap is then given by [25]

$$|\mathbf{B}| = [B_o^2 + (b'r)^2]^{1/2} \approx B_o + \frac{b'^2 r^2}{2B_o}, \tag{2}$$

where the approximation holds for $b'r \ll B_o$. The presence of the $\mathbf{B}_o$ field changes the shape of the potential near the trap center from being linear to harmonic. The interaction potential that follows from Eq. (1) is then, to a good approximation, a harmonic potential of the form $V=V_0+\frac{1}{2}M\omega_r^2 r^2$, where M denotes the mass of the atom. The trap oscillation frequency ω_r is given by

$$\omega_r = \sqrt{\frac{g_F \mu_B m_F}{MB_0}} \frac{\mu_0 I}{2\pi y_0^2}. \tag{3}$$

Moreover, $\mathbf{B}_o$ controls both the splitting of the magnetic sublevels by a frequency $f_0=\frac{1}{2}\mu_B B_o/h$ at the trap center as well as the stability of the resonance associated with the magnetic guide [26].

III. TRAPPING LIFETIMES

In this section, we investigate the two main limitations to the trapping lifetime, thermally induced spin-flip transitions and the Casimir-Polder potential. In the following calculations, we take the current through the single-wall CN to be equal to $I=20$ μA, which seems to be the largest current that can be sustained before saturation effects become important [27]. The physical properties of a CN are determined by the way in which the graphite sheet is rolled. The winding angle with respect to the hexagonal carbon lattice is usually described by two integer numbers (a,b) [28–31]. When $2a+b=3n$, where n is again an integer, a CN shows metallic behavior, otherwise it is semiconducting.

The axial conductivity $\sigma_{zz}(\omega)$ and the resulting dielectric permittivity $\varepsilon(\omega)$ of a (9,0) carbon nanotube are calculated in Appendix A. At a frequency $f_0=70$ kHz, chosen to correspond to an offset field $B_o=10^{-5}$ T=100 mG, we obtain $\sigma_{zz}(\omega_0)=1.19\times10^9+11.5i$ $(\Omega\,\mathrm{m})^{-1}$ and $\varepsilon(\omega_0)\simeq 3\times10^{14}i$. Hence, a (9,0) carbon nanotube can indeed be considered as a metallic cylinder.

Thermal fluctuations generate noise currents that lead to fluctuating fields near the body surface. We expect the noise due to these fluctuating fields to be much reduced in a CN compared to a dielectric bulk material due to the very small amount of matter involved. Nevertheless, thermal spin flips and the Casimir-Polder force cannot be neglected and need investigation and a comparison of their effect. Both mechanisms originate from the fluctuations of the electromagnetic field. In particular, the spin-flip transitions are caused by the magnetic-field fluctuations while the Casimir-Polder force arises from both electric- and magnetic-field fluctuations, the latter usually being negligible.

In order to describe the two phenomena, we utilize the quantization scheme of the electromagnetic field in the presence of dispersing and absorbing bodies [32,33]. As this theory is a macroscopic theory whose central quantities are linear susceptibilities, carbon nanotubes are probably at the limit of what we can actually describe with it. However, when viewed from distances that are several multiples of the bond lengths, the CN can be thought of as a homogeneous object so that the detailed structure from the surface cannot be resolved and QED in dielectrics can be safely used. This also assumes that the CN contains no impurities and shows no pitch alterations.

A. Spin-flip lifetime

If an atom is held sufficiently close to the CN surface it will experience quantum fluctuations of the electromagnetic field. At the center of the trap, the atom experiences a constant magnetic field B_o. The atomic magnetic sublevels are thus split by the Zeeman interaction and only a subset of these levels will experience an attractive force (low-field-seeking states). An ^{87}Rb atom can be trapped in the hyperfine state $|F,m_F\rangle=|2,2\rangle$, but only for sufficiently tight magnetic traps, also in the state $|F,m_F\rangle=|2,1\rangle$. Transitions to lower magnetic sublevels allow the atom to escape. In the following, we disregard all the lower-lying states and treat the atom in the two-level approximation as this transition is the rate-limiting step.

The lifetime of an atom due to spin-flip transitions is given by the inverse of the spin-flip rate [16]

$$\Gamma = \frac{2(\mu_B g_S)^2}{c^2 \varepsilon_0 \hbar} \langle f|\hat{S}_q|i\rangle\langle i|\hat{S}_k|f\rangle \mathrm{Im}[\vec{\boldsymbol{\nabla}} \times \boldsymbol{G}(\mathbf{r},\mathbf{r},\omega_0) \times \overleftarrow{\boldsymbol{\nabla}}]_{qk} \tag{4}$$

where μ_B is the Bohr magneton, $\hat{S}_k$ is the kth vector component of the electronic spin operator, and $g_S \approx 2$ is the electron's g factor. Spin flips occur between the initial state $|i\rangle$ and the final state $|f\rangle$; the position $\mathbf{r}$ of the atom is taken to be the center of the trap.

The spin-flip rate in Eq. (4) is given in terms of the dyadic Green tensor $\boldsymbol{G}(\mathbf{r},\mathbf{r},\omega)$ which contains the physical and geometrical information about the nanotube. We assume the CN to be in thermal equilibrium with the environment at a temperature T. The total spin-flip rate is then given by $\Gamma_{\mathrm{tot}}=\Gamma(\bar{n}_{\mathrm{th}}+1)$, where $\bar{n}_{\mathrm{th}}$ is the mean thermal occupation number $\bar{n}_{\mathrm{th}}=(e^{\hbar\omega_0/k_BT}-1)^{-1}$, with k_B denoting Boltzmann's constant.

In Fig. 1 we show the calculated spin-flip lifetime $\tau_{SF}=1/\Gamma_{\mathrm{tot}}$ as a function of the trapping distance y_0 from the

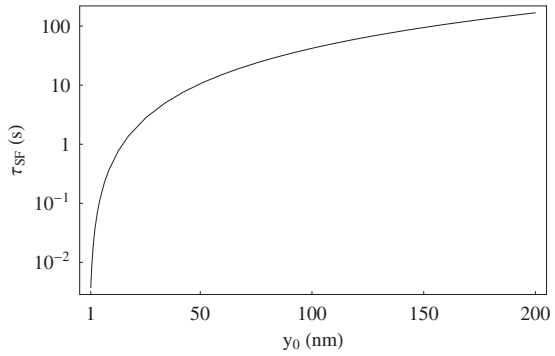

FIG. 1. Spin-flip lifetime of a rubidium atom near a (9, 0) carbon nanotube with radius $R_{CN}=3.52$ Å. The trapping distance y_0 is varied between 1 and 200 nm. The other parameters are $f_0=70$ kHz and $T=380$ K.

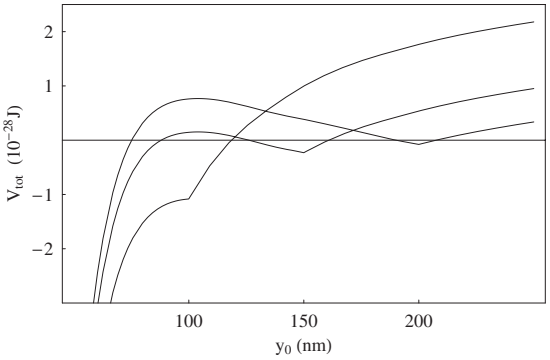

FIG. 2. Potential V_{tot}, the sum of the Casimir-Polder potential of Eq. (5) and the magnetic trapping potential of Eq. (1), for three different trapping distances $y_0=100$, 150, and 200 nm, respectively. A (9,0) CN is considered with a 20 μA current; the spin-flip transition frequency is taken to be $f_0=70$ kHz.

surface of a (9, 0) CN for a temperature $T=380$ K, corresponding to a thermal excitation energy of $k_BT=5.2\times10^{-21}$ J ($\simeq$33 meV). We consider the ground state transition $|2,2\rangle\rightarrow|2,1\rangle$ for an ^{87}Rb atom with the transition frequency $f_0=\omega_0/2\pi=70$ kHz. At such frequencies, the thermally induced spin flips dominate the spontaneous spin flips as $\hbar\omega_0=4.8\times10^{-29}$ J ($\simeq$0.3 neV)$\ll k_BT$. We calculate the spin matrix elements relative to that transition through the Clebsch-Gordan coefficients and obtain for the nonvanishing matrix elements $|\langle i|\hat{S}_x|f\rangle|=|\langle i|\hat{S}_y|f\rangle|=1/4$.

To evaluate the Green tensor that satisfies the correct boundary conditions at the CN surface we used the formulas obtained in Appendix B. In particular, the electric surface current density creates a discontinuity in the tangential component of the magnetic field [34]. To compute the full Green tensor, we use the method of scattering superposition of dyadic Green tensors that are expanded into cylindrical vector wave functions (see, e.g., [35,36]) which somewhat differs from the approach employed in [37].

The lifetime increases with the atom-surface distance y_0 and follows the same power law encountered in [16] for a solid wire. According to Fig. 1, at an atom-surface distance of approximately 20 nm, a lifetime of the order of a few seconds is achievable. The spin-flip lifetime can reach 1 min for distances approaching 120 nm and exceeds more than 100 s for trapping distances larger than 160 nm. These results suggest that an atom can be held very close to a metallic CN for sufficiently long times, and this is in line with our expectations about spin-flip occurrence and with the atom-loss rate estimations presented in [12].

B. Casimir-Polder potential

The presence of macroscopic dielectric bodies changes drastically the structure of the vacuum electromagnetic field. One consequence is that an atom in its ground state placed sufficiently close to a dielectric body experiences a nonvanishing, in general attractive, dispersion force, the Casimir-Polder (CP) force [20,38–40]. Since the CP potential adds to the (repulsive) trapping potential, atoms can tunnel through the resulting potential barrier and get stuck at the nanotube surface. The lifetime we have calculated in Sec. III A provides information about the distance at which an atom can be held before thermally driven spin flips occur in a given time, but the Casimir-Polder force may play an even bigger role for small enough distances.

The Casimir-Polder potential can be derived in lowest-order perturbation theory within the framework of QED in dielectric media [39]. If we assume that an atom is in an energy eigenstate $|l\rangle$, then the CP potential is given by the body-induced—i.e., dependent on the quantity of material—(and position-dependent) shift of the eigenvalue ΔE_l corresponding to this eigenstate $|l\rangle$. The CP potential can be expressed as [20,39]

$$U(\mathbf{r})=\frac{\hbar\mu_0}{2\pi}\int_0^\infty du\, u^2\alpha_l^{(0)}(iu)\mathrm{Tr}[\boldsymbol{G}^{(S)}(\mathbf{r},\mathbf{r},iu)] \tag{5}$$

where $iu=\omega$ and $\alpha_l^{(0)}(\omega)$ is the atomic polarizability in lowest-order perturbation theory. In particular, for an atom in a spherically symmetric ground state, one finds that

$$\alpha_l^{(0)}(\omega)=\lim_{\xi\rightarrow0}\frac{2}{3\hbar}\sum_k\frac{\omega_{kl}}{\omega_{kl}^2-\omega^2-i\omega\xi}|\mathbf{d}_{lk}|^2 \tag{6}$$

with $\mathbf{d}_{lk}=\langle l|\hat{\mathbf{d}}|k\rangle$ representing the matrix dipole elements relative to the transition from the atomic initial state $|l\rangle$ to the allowed states $|k\rangle$ with frequency $\omega_{kl}\equiv(E_k-E_l)/\hbar$. The expression of the CP potential in Eq. (5) is given in terms of the scattering part $\boldsymbol{G}^{(S)}(\mathbf{r},\mathbf{r},iu)$ of the Green tensor and the frequency integral is performed along the imaginary axis.

The Casimir-Polder potential has to be compared with the magnetic trapping potential in order to establish the size of its effect. In Fig. 2 we show V_{tot}, the total potential experienced by the atom at three different trapping distances $y_0=100$, 150, and 200 nm. V_{tot} is given by the sum of the two potentials defined by Eqs. (1) and (5). We assume that a 20 μA current is flowing through the CN, and the associated heating justifies our choice of the temperature to be significantly higher than room temperature. Among all the possible transitions $|l\rangle\rightarrow|k\rangle$, we consider only the lowest electronic transition $D_2(5\,^2S_{1/2}\rightarrow5\,^2P_{3/2})$ with wavelength $\lambda\simeq780$ nm and dipole moment $|\mathbf{d}_2|=4.227ea_0$ (a_0 is the classical Bohr

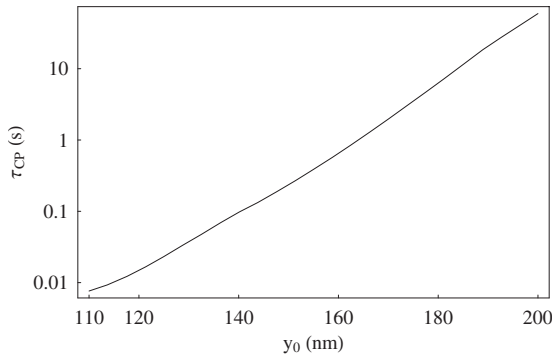

FIG. 3. Tunneling time τ_{CP} as a function of the trapping distance y_0, varied between 110 and 200 nm.

radius). We assume that the D_2 transition represents the main contribution to the atomic polarizability, while other transitions bring about a negligible contribution to the CP force.

In contrast to the spin-flip lifetime, temperature effects are negligible here because $hc/\lambda = 2.5 \times 10^{-19}$ J ($\simeq 1.6$ eV) $\gg k_B T$. This means that the resonant contributions corresponding to virtual dipole absorption [41] are suppressed. It also allows us to replace the Matsubara sum by the integral in Eq. (5) which effectively has to be computed over a frequency range set by hc/λ.

As it is evident from Fig. 2, V_{tot} forms a potential barrier whose height and width vary with the trapping distance y_0. As mentioned previously, the addition of the offset field $\mathbf{B}_o$ changes the bottom of the potential well from a linear to a harmonic trap which is, however, not visible on the scale of the figure. With decreasing y_0 the potential barrier becomes more and more shallow, until for atom-surface distances smaller than the critical value of $y_0 \simeq 100$ nm the barrier effectively disappears. For trapping distances larger than that, the total potential shows a pronounced minimum. For example, for $y_0 = 150$ nm we estimate the trap oscillation frequency to be $\omega_r \simeq 0.7$ kHz, and the width and the height of the potential barrier to be 68.6 nm and 3.8×10^{-29} J, respectively.

Using the WKB approximation, we can estimate the tunneling probability T and the corresponding tunneling lifetime $\tau_{CP} = 2\pi/(T\omega_r)$. The result is shown in Fig. 3 for a ground-state atom trapped at varying distances y_0. From the comparison of Fig. 1 and Fig. 3, it is clear that the effect of the CP force cannot be neglected. For small enough atom-nanotube distances (and indeed for all distances shown in the figures) the tunneling lifetime is several orders of magnitude smaller than the spin-flip lifetime. For example, at a trapping distance $y_0 = 150$ nm we estimate τ_{SF} and τ_{CP} to be 94.4 and 0.2 s, respectively, and a tunneling lifetime of a few seconds is achievable for trapping distances equal to or bigger than 170 nm, where the spin-flip occurrence is no longer a limiting factor.

IV. CONCLUSION

In this paper we have investigated a method of miniaturizing atomic magnetic traps by replacing solid current-carrying wires with carbon nanotubes as the elementary building blocks. At first sight, the advantages of using CNs are both their small diameter and the fact that they are effectively two-dimensional structures. Hence, one would expect from scaling arguments that traps at rather small atom-surface distances could be realized.

We have investigated the loss mechanisms both due to thermally induced spin flips as well as by tunneling through the Casimir-Polder barrier. The calculations have been performed within the framework of quantum electrodynamics in dielectric media, which is valid as long as the dielectric properties of the nanotube can be described by a macroscopic permittivity, and if the experimental situation is such that the atomic structure of the CN cannot be resolved and macroscopic boundary conditions can be set.

The spin-flip lifetime has been found to scale according to our expectations. That is, this lifetime follows, as a function of the atom-surface distance, the same power law as in the case of a solid wire, with the result that for distances much larger than the radius of the nanotube the expected lifetime exceeds several seconds. In contrast, the alterations of the trapping potential by the Casimir-Polder potential are much more severe. It appears that the minimal feasible trapping distance is larger than 100 nm. The main reason explaining this result is that single-wall nanotubes cannot sustain high enough currents (and thus cannot generate deep enough magnetic traps) as they saturate at high electric fields. As a potential remedy, it would be beneficial to consider multiwall nanotubes. An increased number of carbon layers would allow for higher current densities and consequently a magnetic trapping potential that would be comparable with the Casimir-Polder potential even for smaller distances.

ACKNOWLEDGMENTS

We wish to thank Lene V. Hau who, after an initial discussion, stimulated our interest in this subject. This work was supported by the U.K. Engineering and Physical Sciences Research Council (EPSRC), partly through the UK Quantum Information Processing Interdisciplinary Research Collaboration (QIP IRC), and the CONQUEST and SCALA programs of the European commission.

APPENDIX A: AXIAL CONDUCTIVITY AND DIELECTRIC PERMITTIVITY

The calculation of the Casimir-Polder potential requires full knowledge of the frequency dependence of the conductivity. In order to make our presentation self-contained we quote some results on calculations of the axial conductivity that have previously been published elsewhere.

Here we briefly review the frequency dependence of the axial surface conductivity $\sigma_{zz}(\omega)$ and of the dielectric permittivity $\varepsilon(\omega)$ for a single-wall CN following the presentation in [29,30]. For a dielectric medium, the linear relation between $\sigma(\omega)$ and $\varepsilon(\omega)$ is $\varepsilon(\omega)/\varepsilon_0 - 1 = i\sigma(\omega)/(\omega\varepsilon_0)$, where $\varepsilon_r(\omega) = \varepsilon(\omega)/\varepsilon_0$ is the (complex) relative dielectric permittivity. The Clausius-Mosotti equation establishes the relation between the response of a medium to an applied field, i.e., the polarization, and its dielectric constant. Because of the cylin-

drical structure of CNs, their polarizability is highly anisotropic, with the principal axis of the polarizability tensor oriented parallel to the cylindrical axis [14,29,42–44]. Consequently, one is allowed to neglect the azimuthal current [45]. The axial conductivity per unit length can be expressed as [29,37]

$$\sigma_{zz}(\mathbf{R},\omega) = -\frac{i\omega\varepsilon_0}{S}\frac{\varepsilon_r(\mathbf{R},\omega)-1}{\rho_T} \tag{A1}$$

where $\mathbf{R}=(\mathrm{R}_{CN},\phi,Z)$ is the radius vector of an arbitrary point of the CN surface, S is the area of a single nanotube, and ρ_T is the tubule density in a bundle.

The physical properties of a CN are determined by the way in which the graphite sheet is rolled. The winding angle with respect to the hexagonal carbon lattice is usually described by two integer numbers (a,b). Depending on a and b, CNs are either semiconducting or metallic, and particularly a CN exhibits metallic properties when $2a+b=3n$, where n is again an integer [28–31]. An (a,b) CN has a one-dimensional bands

$$E_{\pm}(N,p) = \pm t_0 \times \sqrt{1+4\cos\left(\frac{2\pi N}{a}-\frac{a+2b}{2a}p\ell\right)\cos\frac{p\ell}{2}+4\cos^2\frac{p\ell}{2}}$$

where ℓ is $\frac{3}{2}$ times the interatomic distance, $N=0,1,\ldots,a-1$, and $\pi/\ell \leqslant p \leqslant \pi/\ell$ with p the wave number. The corresponding Fermi distribution function is $f(E)=1/\{\exp[\beta(E-\mu)]+1\}$ with inverse temperature β and chemical potential μ.

The main contribution to the conductivity is given by the dynamic conductivity due to the free carrier term $\varepsilon_r^f(\omega)$ but for high-frequency regimes another term $\varepsilon_r^b(\omega)$, arising from the transition between the conduction and the valence bands, becomes important such that the relative dielectric permittivity is given by $\varepsilon_r(\omega)=\varepsilon_r^f(\omega)+\varepsilon_r^b(\omega)$ [29,45]. The interband transition term is given by

$$\varepsilon_r^b(\omega) = 1+\left(\frac{e\hbar^2}{m}\right)^2\frac{4\rho c}{a\ell}\sum_N \times \int_{-\pi/l}^{\pi/l} dp\frac{f(E_+(N,p))-f(E_-(N,p))}{E_+(N,p)-E_-(N,p)} \times \frac{[\mathrm{Re}\,K_0(N,p)]^2}{(\hbar\omega)^2+i\hbar^2\omega/\tau_r-[E_+(N,p)-E_-(N,p)]^2}, \tag{A2}$$

where τ_r is a phenomenological relaxation time and $\rho_C=2a\rho_T=(\pi\sqrt{3})/(2R_{\mathrm{CN}}\ell^2)$ is the density of carbon atoms per volume [31]. The Drude term is given by

$$\varepsilon_r^f(\omega) = -\frac{(\hbar\omega_{pl})^2}{\hbar\omega(\hbar\omega+i\hbar/\tau_r)}, \tag{A3}$$

with ω_{pl} the plasma frequency,

$$\omega_{pl}^2 = -\left(\frac{e\hbar}{m}\right)^2\frac{2\rho_C}{a\ell}\sum_N\int_{-\pi/\ell}^{\pi/\ell} dp[\mathrm{Im}\,K_0(N,p)]^2 \times [f'(E_+(N,p))+f'(E_-(N,p))]. \tag{A4}$$

The quantity $K_0(N,p)$ corresponds to the (dimensionless) matrix element of the momentum operator and is given in [29]. The following parameters have been used in our calculations: $t_0=4.32\times10^{-19}$ J, $\hbar/\tau_r=4.8\times10^{-21}$ J, $\ell=2.13$ Å, $R_{CN}=3.52$ Å.

APPENDIX B: GREEN TENSOR OF A SINGLE-WALL CARBON NANOTUBE

In this section we present our calculation of the dyadic Green tensor for a single-wall CN. For a single-wall nanotube, we can approximate the carbon layer by a boundary layer with zero thickness. In this way, the Green tensor exhibits a discontinuity in its first spatial derivative across the carbon layer. Due to its cylindric symmetry, the problem can be described by adopting the cylindric basis $\{\mathbf{e}_r,\mathbf{e}_\varphi,\mathbf{e}_z\}$ assuming the CN to be directed along $\mathbf{e}_z$. We use the method of scattering superposition (see, e.g., [35,36]). For an atom located at $\mathbf{r}'$ outside the CN, the Green tensor can thus be written as

$$\boldsymbol{G}(\mathbf{r},\mathbf{r}',\omega) = \begin{cases} \boldsymbol{G}_0(\mathbf{r},\mathbf{r}',\omega)+\boldsymbol{G}_R^{(S)}(\mathbf{r},\mathbf{r}',\omega), & r>R_{CN}, \\ \boldsymbol{G}_T^{(S)}(\mathbf{r},\mathbf{r}',\omega), & r<R_{CN}, \end{cases} \tag{B1}$$

where $\boldsymbol{G}_0(\mathbf{r},\mathbf{r}',\omega)$ is the unbounded (bulk) Green tensor representing the contribution of direct waves from the source at $\mathbf{r}'$ to the point $\mathbf{r}$, and the two scattering contributions $\boldsymbol{G}_R^{(S)}(\mathbf{r},\mathbf{r}',\omega)$ and $\boldsymbol{G}_T^{(S)}(\mathbf{r},\mathbf{r}',\omega)$ describing the reflection and transmission of waves from and through the cylindrical surface. In order to satisfy the homogeneous Helmholtz equation and the radiation condition at infinity, the vacuum term and the two scattering terms can be taken to be in the following forms [36]:

$$\boldsymbol{G}_0(\mathbf{r},\mathbf{r}',\omega) = -\frac{\hat{\mathbf{r}}\hat{\mathbf{r}}\,\delta(\mathbf{r}-\mathbf{r}')}{k^2}+\frac{i}{8\pi}\int_{-\infty}^{\infty}dh\sum_{n=0}^{\infty}\frac{2-\delta_{n0}}{\eta^2} \times \begin{cases} \mathbf{M}_{{}^{e}_{o}n}^{(1)}(h)\mathbf{M}_{{}^{e}_{o}n}'(-h)+\mathbf{N}_{{}^{e}_{o}n}^{(1)}(h)\mathbf{N}_{{}^{e}_{o}n}'(-h), & r>r', \\ \mathbf{M}_{{}^{e}_{o}n}(h)\mathbf{M}_{{}^{e}_{o}n}'^{(1)}(-h)+\mathbf{N}_{{}^{e}_{o}n}(h)\mathbf{N}_{{}^{e}_{o}n}'^{(1)}(-h), & r<r', \end{cases} \tag{B2}$$

$$\boldsymbol{G}_R^{(S)}(\mathbf{r},\mathbf{r}',\omega) = \frac{i}{8\pi}\int_{-\infty}^{\infty}dh\sum_{n=0}^{\infty}\frac{2-\delta_{n0}}{\eta^2} \times \{[\mathcal{C}_{1H}\mathbf{M}_{{}^{e}_{o}n}^{(1)}(h)+\mathcal{C}_{2H}\mathbf{N}_{{}^{o}_{e}n}^{(1)}(h)]\mathbf{M}_{{}^{e}_{o}n}'^{(1)}(-h) +[\mathcal{C}_{1V}\mathbf{N}_{{}^{e}_{o}n}^{(1)}(h)+\mathcal{C}_{2V}\mathbf{M}_{{}^{o}_{e}n}^{(1)}(h)]\mathbf{N}_{{}^{e}_{o}n}'^{(1)}(-h)\}, \tag{B3}$$

$$\boldsymbol{G}_T^{(S)}(\mathbf{r},\mathbf{r}',\omega) = \frac{i}{8\pi}\int_{-\infty}^{\infty} dh \sum_{n=0}^{\infty} \frac{2-\delta_{n0}}{\eta^2} \times \{[\mathcal{C}_{3H}\mathbf{M}_{\substack{e_n \\ o}}(h) + \mathcal{C}_{4H}\mathbf{N}_{\substack{o_n \\ e}}(h)]\mathbf{M}'^{(1)}_{\substack{e_n \\ o}}(-h) + [\mathcal{C}_{3V}\mathbf{N}_{\substack{e_n \\ o}}(h) + \mathcal{C}_{4V}\mathbf{M}_{\substack{o_n \\ e}}(h)]\mathbf{N}'^{(1)}_{\substack{e_n \\ o}}(-h)\}, \tag{B4}$$

where $k=\omega/c$ and $\eta^2=k^2-h^2$. To enhance readability, we have omitted the tensor product symbol $\otimes$ between the even (e) and odd (o) cylindrical vector wave functions, which are defined as

$$\mathbf{M}_{\substack{e_n \\ o}}(h) = \boldsymbol{\nabla} \times \left[Z_n(\eta r)\begin{pmatrix}\cos \\ \sin\end{pmatrix} n\phi\, e^{ihz}\mathbf{e}_z \right], \tag{B5}$$

$$\mathbf{N}_{\substack{e_n \\ o}}(h) = \frac{1}{k}\boldsymbol{\nabla} \times \boldsymbol{\nabla} \times \left[Z_n(\eta r)\begin{pmatrix}\cos \\ \sin\end{pmatrix} n\phi\, e^{ihz}\mathbf{e}_z \right]. \tag{B6}$$

The symbol $Z_n(x)$ has to be replaced either by the Bessel function $J_n(x)$ or, if the superscript (1) appears on the corresponding vector wave function, by the (outgoing) Hankel function of the first kind, $H_n^{(1)}(x)$. The primes in Eqs. (B2)–(B4) indicate the cylindrical coordinates (r',ϕ',z'). The coefficients $\mathcal{C}_{mP}$ ($m=1$, 2, 3, and 4, and $P=H$, V) need to be determined from the boundary conditions for the electric- and magnetic-field components on the CN surface. The electric field satisfies the boundary condition

$$\mathbf{e}_r \times [\,\mathbf{E}(\mathbf{r},\omega)|_{r=R_{CN}^+} - \mathbf{E}(\mathbf{r},\omega)|_{r=R_{CN}^-}] = 0, \tag{B7}$$

while the electric surface current density creates a discontinuity in the tangential component of the magnetic field,

$$\mathbf{e}_r \times [\,\mathbf{H}(\mathbf{r},\omega)|_{r=R_{CN}^+} - \mathbf{H}(\mathbf{r},\omega)|_{r=R_{CN}^-}] = \mathbf{J}(\mathbf{r},\omega)|_{r=R_{CN}}. \tag{B8}$$

Equations (B7) and (B8) translate into the respective boundary conditions for the Green tensor

$$\mathbf{e}_r \times [\,\boldsymbol{G}(\mathbf{r},\mathbf{r}',\omega)|_{r=R_{CN}^+} - \boldsymbol{G}(\mathbf{r},\mathbf{r}',\omega)|_{r=R_{CN}^-}] = 0, \tag{B9}$$

$$\mathbf{e}_r \times \boldsymbol{\nabla} \times [\,\boldsymbol{G}(\mathbf{r},\mathbf{r}',\omega)|_{r=R_{CN}^+} - \boldsymbol{G}(\mathbf{r},\mathbf{r}',\omega)|_{r=R_{CN}^-}] = i\omega\mu_0\boldsymbol{\sigma}(\mathbf{r})\cdot\boldsymbol{G}(\mathbf{r},\mathbf{r}',\omega)|_{r=R_{CN}}, \tag{B10}$$

where $\boldsymbol{\sigma}(\mathbf{r})$ is the (diagonal) conductivity tensor whose only nonzero element is $\sigma_{zz}(\mathbf{R},\omega)$.

Substituting the decomposition (B1), together with Eqs. (B2)–(B4), into the boundary conditions (B9) and (B10) leads to two sets of four equations for each polarization H and V, which enable us to determine the 16 coefficients $\mathcal{C}_{mP}$,

$$-\frac{\eta^2}{k}H_n(\eta r)\mathcal{C}_{2H} + \frac{\eta^2}{k}J_n(\eta r)\mathcal{C}_{4H} = 0, \tag{B11}$$

$$-\partial_r H_n(\eta r)\mathcal{C}_{1H} \pm \frac{ihn}{kr}H_n(\eta r)\mathcal{C}_{2H} + \partial_r J_n(\eta r)\mathcal{C}_{3H} \mp \frac{ihn}{kr}J_n(\eta r)\mathcal{C}_{4H} = \partial_r J_n(\eta r), \tag{B12}$$

$$-\eta^2 H_n(\eta r)\mathcal{C}_{1H} + \eta^2 J_n(\eta r)\mathcal{C}_{3H} = \eta^2 J_n(\eta r), \tag{B13}$$

$$\mp\frac{ihn}{r}H_n(\eta r)\mathcal{C}_{1H} - k\partial_r H_n(\eta r)\mathcal{C}_{2H} \pm \frac{ihn}{r}J_n(\eta r)\mathcal{C}_{3H} + \left(k\partial_r J_n(\eta r) - i\omega\mu_0\sigma_{zz}\frac{\eta^2}{k}J_n(\eta r)\right)\mathcal{C}_{4H} = \pm\frac{ihn}{r}J_n(\eta r) \tag{B14}$$

and

$$-\frac{\eta^2}{k}H_n(\eta r)\mathcal{C}_{1V} + \frac{\eta^2}{k}J_n(\eta r)\mathcal{C}_{3V} = \frac{\eta^2}{k}J_n(\eta r), \tag{B15}$$

$$\mp\frac{ihn}{kr}H_n(\eta r)\mathcal{C}_{1V} - \partial_r H_n(\eta r)\mathcal{C}_{2V} \pm \frac{ihn}{kr}J_n(\eta r)\mathcal{C}_{3V} + \partial_r J_n(\eta r)\mathcal{C}_{4V} = \pm\frac{ihn}{kr}J_n(\eta r), \tag{B16}$$

$$-\eta^2 H_n(\eta r)\mathcal{C}_{2V} + \eta^2 J_n(\eta r)\mathcal{C}_{4V} = 0, \tag{B17}$$

$$-k\partial_r H_n(\eta r)\mathcal{C}_{1V} \pm \frac{ihn}{r}H_n(\eta r)\mathcal{C}_{2V} + \left(k\partial_r J_n(\eta r) - i\omega\mu_0\sigma_{zz}\frac{\eta^2}{k}J_n(\eta r)\right)\mathcal{C}_{3V} \mp \frac{ihn}{r}J_n(\eta r)\mathcal{C}_{4V} = k\partial_r J_n(\eta r). \tag{B18}$$

The appearance of the axial conductivity $\sigma_{zz}(\mathbf{R},\omega)$ in the boundary conditions (B14) and (B18) reflects the jump condition (B10) of the derivative of the Green tensor at the boundary layer.

As we need to compute only the Green function in the region where the atom is located, only $\mathcal{C}_{(1,2)P}$ need to be determined. On using various properties of the Bessel functions such as the Wronskian between the Bessel function $J_n(x)$ and the Hankel function $H_n^{(1)}(x)$, $J_n(x)H_n^{(1)\prime}(x) - J_n'(x)H_n^{(1)}(x) = 2/(\pi x)$, we obtain that the only nonzero coefficient is

$$\mathcal{C}_{1V} = -\frac{\pi\mu_0\omega R_{CN}\sigma_{zz}\eta^2 J_n^2(\eta R_{CN})}{2k^2 + \pi\mu_0\omega R_{CN}\sigma_{zz}\eta^2 J_n(\eta R_{CN})H_n(\eta R_{CN})} \tag{B19}$$

Finally, the Green tensor for an atom located at a position $\mathbf{r}'$ outside the CN can be expressed as

$$\boldsymbol{G}(\mathbf{r},\mathbf{r}',\omega) = \boldsymbol{G}_0(\mathbf{r},\mathbf{r}',\omega) + \frac{i}{8\pi}\int_{-\infty}^{\infty} dh \sum_{n=0}^{\infty} \frac{2-\delta_{n0}}{\eta^2} \times \mathcal{C}_{1V}\mathbf{N}^{(1)}_{\substack{e_n \\ o}}(h)\mathbf{N}'^{(1)}_{\substack{e_n \\ o}}(-h). \tag{B20}$$

Equation (B20), together with Eq. (B2), is the expression for the Green tensor used throughout this paper.

[1] E. A. Hinds and I. G. Hughes, J. Phys. D **32**, R119 (1999).
[2] W. Hänsel, P. Hommelhoff, T. W. Hänsch, and J. Reichel, Nature (London) **413**, 408 (2001).
[3] R. Folman, P. Krüger, J. Schmiedmayer, J. Denschlag, and C. Henkel, Adv. At., Mol., Opt. Phys. **48**, 263 (2002).
[4] J. Reichel, Appl. Phys. B: Lasers Opt. **75**, 469 (2002).
[5] C. Henkel, K. Joulain, R. Carminati, and J.-J. Greffet, Opt. Commun. **186**, 57 (2000).
[6] M. P. A. Jones, C. J. Vale, D. Sahagun, B. V. Hall, C. C. Eberlein, B. E. Sauer, K. Furusawa, D. Richardson, and E. A. Hinds, J. Phys. B **37**, L15 (2004).
[7] R. Fermani, S. Scheel, and P. L. Knight, Phys. Rev. A **73**, 032902 (2006).
[8] J. Schmiedmayer, R. Folman, and T. Calarco, J. Mod. Opt. **49**, 1375 (2002).
[9] D. Jaksch, Contemp. Phys. **45**, 367 (2004).
[10] S. Wildermuth, S. Hofferberth, I. Lesannovsky, E. Haller, L. M. Andersson, S. Groth, I. Bar-Joseph, P. Krüger, and J. Schmiedmayer, Nature (London) **435**, 440 (2005).
[11] S. Wildermuth, S. Hofferberth, I. Lesannovsky, E. Haller, L. M. Andersson, S. Groth, I. Bar-Joseph, P. Krüger, and J. Schmiedmayer, Appl. Phys. Lett. **88**, 264103 (2006).
[12] V. Peano, M. Thorwart, A. Kasper, and R. Egger, Appl. Phys. B **81**, 1075 (2005).
[13] S. Iijima, Nature (London) **354**, 56 (1994).
[14] L. X. Benedict, S. G. Louie, and M. L. Cohen, Phys. Rev. B **52**, 8541 (1995).
[15] C. Henkel, S. Pötting, and M. Wilkens, Appl. Phys. B: Lasers Opt. **69**, 379 (1999).
[16] P. K. Rekdal, S. Scheel, P. L. Knight, and E. A. Hinds, Phys. Rev. A **70**, 013811 (2004).
[17] M. P. A. Jones, C. J. Vale, D. Sahagun, B. V. Hall, and E. A. Hinds, Phys. Rev. Lett. **91**, 080401 (2003).
[18] D. M. Harber, J. M. McGuirk, J. M. Obrecht, and E. A. Cornell, J. Low Temp. Phys. **133**, 229 (2003).
[19] Y. J. Lin, I. Teper, C. Chin, and V. Vuletić, Phys. Rev. Lett. **92**, 050404 (2004).
[20] I. E. Dzyaloshinskii, E. M. Lifshitz, and L. P. Pitaevskii, Adv. Phys. **10**, 165 (1961).
[21] P. W. Milonni, *The Quantum Vacuum: An Introduction to Quantum Electrodynamics* (Academic Press, London, 1994).
[22] E. V. Blagov, G. L. Klimchitskaya, and V. M. Mostepanenko, Phys. Rev. B **71**, 235401 (2005).
[23] J. M. Obrecht, R. J. Wild, M. Antezza, L. P. Pitaevskii, S. Stringari, and E. A. Cornell, Phys. Rev. Lett. **98**, 063201 (2007).
[24] J. Reichel, Appl. Phys. B: Lasers Opt. **75**, 469 (2002).
[25] C. J. Foot, *Atomic Physics* (Oxford University Press, Oxford, 2005).
[26] J. Bill, Martin-I. Trappe, I. Lesanovsky, and P. Schmelcher, Phys. Rev. A **73**, 053609 (2006).
[27] Z. Yao, C. L. Kane, and C. Dekker, Phys. Rev. Lett. **84**, 2941 (2000).
[28] N. Hamada, S. I. Sawada, and A. Oshiyama, Phys. Rev. Lett. **68**, 1579 (1992).
[29] S. Tasaki, K. Maekawa, and T. Yamabe, Phys. Rev. B **57**, 9301 (1998).
[30] M. F. Lin and Kenneth W.-K. Shung, Phys. Rev. B **50**, 17744 (1994).
[31] H. Jiang, G. Wu, X. Yang, and J. Dong, Phys. Rev. B **70**, 125404 (2004).
[32] S. Scheel, L. Knöll, and D.-G. Welsch, Phys. Rev. A **58**, 700 (1998).
[33] L. Knöll, S. Scheel, and D.-G. Welsch, in *Coherence and Statistics of Photons and Atoms*, edited by J. Peřina (Wiley, New York, 2001).
[34] G. Y. Slepyan, S. A. Maksimenko, A. Lakhtakia, O. M. Yevtushenko, and A. V. Gusakov, Phys. Rev. B **57**, 9485 (1998).
[35] W. C. Chew, *Waves and Fields in Inhomogeneous Media* (IEEE Press, New York, 1995).
[36] L.-W. Li, M.-S. Leong, T.-S. Yeo, and P.-S. Kooi, J. Electromagn. Waves Appl. **14**, 961 (2000).
[37] I. V. Bondarev and Ph. Lambin, Phys. Rev. B **70**, 035407 (2004).
[38] H. B. G. Casimir and D. Polder, Phys. Rev. **73**, 360 (1947).
[39] S. Y. Buhmann, L. Knöll, D.-G. Welsch, and H. T. Dung, Phys. Rev. A **70**, 052117 (2004).
[40] S. Y. Buhmann, T. D. Ho, and D.-G. Welsch, J. Opt. B: Quantum Semiclassical Opt. **6**, S127 (2004).
[41] M.-P. Gorza and M. Ducloy, Eur. Phys. J. D **40**, 343 (2006).
[42] Z. M. Li, Z. K. Tang, H. J. Liu, N. Wang, C. T. Chan, R. Saito, S. Okada, G. D. Li, J. S. Chen, N. Nagasawa, and S. Tsuda, Phys. Rev. Lett. **87**, 127401 (2001).
[43] A. Jorio, A. G. Souza Filho, V. W. Brar, A. K. Swan, M. S. Ünlü, B. B. Goldberg, A. Righi, J. H. Hafner, C. M. Lieber, R. Saito, G. Dresselhaus, and M. S. Dresselhaus, Phys. Rev. B **65**, 121402(R) (2002).
[44] A. G. Marinopoulos, L. Reining, A. Rubio, and N. Vast, Phys. Rev. Lett. **91**, 046402 (2003).
[45] G. Ya. Slepyan, S. A. Maksimenko, A. Lakhtakia, O. Yevtushenko, and A. V. Gusakov, Phys. Rev. B **60**, 17136 (1999).